Journal of Oceanography, Vol. 58, pp. 477 to 486, 2002

Probability Distribution of Surface Wave Slope Derived Using Sun Glitter Images from Geostationary Meteorological Satellite and Surface Vector Winds from Scatterometers

NAOTO EBUCHI[1]* and SHOICHI KIZU[2]

[1]*Center for Atmospheric and Oceanic Studies, Graduate School of Science, Tohoku University, Aoba, Sendai 980-8578, Japan*
[2]*Department of Geophysics, Graduate School of Science, Tohoku University, Aoba, Sendai 980-8578, Japan*

(Received 29 June 2001; in revised form 15 October 2001; accepted 29 October 2001)

The probability distribution of the sea surface slope has been estimated using sun glitter images derived from the visible wavelength radiometer on the Geostationary Meteorological Satellite (GMS) and surface vector winds observed by spaceborne scatterometers. The brightness of the visible images is converted to the probability of wave surfaces which reflect the sunlight toward GMS in grids of 0.25° × 0.25° (latitude × longitude). The slope and azimuth angle required for the reflection of the sun's rays toward GMS are calculated for each grid from the geometry of GMS observation and location of the sun. The GMS images are then collocated with surface wind data observed by three scatterometers. Using the collocated data set of about 30 million points obtained in a period of 4 years from 1995 to 1999, the probability distribution function of the surface slope is estimated as a function of wind speed and azimuth angle relative to the wind direction. The results are compared with those of Cox and Munk (1954a). The surface slope estimated by the present method shows a narrower distribution and much less directivity relative to the wind direction than that reported by Cox and Munk. It is expected that their data were obtained under conditions of growing wind waves. In general, wind waves are not always developing, and the slope distribution might differ from the results of Cox and Munk. Most of our data are obtained in the subtropical seas under clear-sky conditions. This difference in the conditions may be the reason for the difference of slope distribution.

Keywords:
· Wind waves,
· surface slope,
· sun glitter,
· scatterometer,
· Geostationary Meteorological Satellite,
· visible radiometer.

1. Introduction

The distribution of the sea surface slopes is of broad interest not only for the physics of wind waves and wave modeling but also for optical models of the ocean surface and ocean color remote sensing. Almost a half century ago, Cox and Munk (1954a, b) derived the probability distribution of surface slope from aerial photographs of the sun's glitter on the sea surface. Their relationship between variance of the surface slope and wind speed has been widely used to model the optical properties of the sea surface. However, their results were deduced from a very limited number of photographs taken under selected conditions.

* Corresponding author. E-mail: ebuchi@ocean.caos.tohoku.ac.jp

The surface slope distribution has been measured by several investigators in laboratories (e.g., Wu, 1971; Long and Huang, 1976) and at observation towers in the ocean (e.g., Hughes *et al.*, 1977; Tang and Shemdin, 1983; Hwang and Shemdin, 1988). Some systematic deviations from the relationship between the slope variance and wind speed proposed by Cox and Munk (1954a, b) were reported in these studies. It was pointed out that the distribution of the sea surface slope may depend not only on the wind speed but on the other environmental conditions such as atmospheric stability and swells (Hwang and Shemdin, 1988). However, field observations of the sea surface slope have been very limited in geographical coverage and range of environmental conditions because of difficulties in making accurate measurements.

Spacecraft observations of sun glitter have also been used to investigate the relationship between the surface

slope distribution and wind speed (e.g., Soules, 1970; Strong and Ruff, 1970; Levanon, 1971; Wylie *et al*., 1981; Wald and Monget, 1983; Khattak *et al*., 1991). In these studies, however, only a few snapshots were analyzed and the results were compared qualitatively with those of Cox and Munk (1954a, b). Statistical analysis has been hampered by the huge data amount of the satellite visible images.

In the present study we have attempted to estimate the probability distribution of the sea surface slope as a function of wind speed and azimuth angle relative to the wind direction using sun glitter images observed by the Geostationary Meteorological Satellite (GMS) and surface vector winds derived from spaceborne scatterometers, such as the European Remote sensing Satellite (ERS)-1 and -2/Active Microwave Instrument (AMI), and ADvanced Earth Observation Satellite (ADEOS)/National Astronautics and Space Administration (NASA) Scatterometer (NSCAT). High-speed processing of the GMS data enabled us to obtain a collocated data set for a period of 4.5 years. It is expected that we shall be able to derive a more reliable probability density function under general conditions of wind and waves over the global oceans. Since our data set is obtained under clear-sky conditions with a resolution of an order of 10 km, our results are expected to be directly applicable to optical modeling of the sea surface for ocean color remote sensing.

2. Data and Method

2.1 Data

We used the GMS-5/Visible and Infrared Spin Scan Radiometer (VISSR) Histogram Data (Meteorological Satellite Center, 1989) provided by the Japan Meteorological Agency (JMA) for a period of about 4 years from June 14, 1995 to September 30, 1999. The data cover an area of latitude between 60°S and 60°N, and longitude between 80°E and 160°W, with temporal interval of 3 hours. The data store histograms of pixel-wise visible brightness count in grids of $0.25° \times 0.25°$ (latitude $\times$ longitude).

The NSCAT Ocean Wind Products (Level 2.0) provided by the NASA Physical Oceanography Distributed Active Archive Center (PO.DAAC) at the Jet Propulsion Laboratory (JPL), California Institute of Technology, and the ERS-1/2 AMI Off-line Wind Scatterometer Products provided by Centre ERS d'Archivage et de Traitement (CERSAT), Institut Français de Recherche pour l'Exploitation de la Mer (IFREMER), were utilized to collocate with the GMS data. The ERS-1, ERS-2, and NSCAT wind data products cover periods from June 14, 1995 to May 25, 1996, from March 19, 1996 to September 30, 1999, and from September 15, 1996 to June 30, 1997, respectively. NSCAT had two 600 km-wide swaths on the both sides of satellite subtrack, and ERS-1 and -2 had a 500 km-wide swath on the right side only. The spatial resolution of these wind products is 50 km, although the spacing of the ERS wind products is 25 km. The scatterometers are considered to provide with the equivalent neutral wind at a height of 10 m above the sea surface. Several validation studies of these products (e.g., Bentamy *et al*., 1994; Quilfen and Bentamy, 1994; Ebuchi *et al*., 1996, 1998; Graber *et al*., 1996; Freilich and Dunbar, 1999; Masuko *et al*., 2000) reported that accuracies of the wind speed and direction observed by these scatterometers are about 2 ms^{-1} and 20°, respectively.

Fig. 1. Example of GMS visible image (0300 UT, June 28, 1995).

2.2 Method

Figure 1 shows an example of a GMS-5/VISSR visible image which contains sun glitter in the sea north of Australia. The brightness of the visible images is converted to the probability of wave surfaces which reflects the sunlight toward GMS. Figure 2 is a flowchart of the data processing.

Visible brightness counts of all pixels are averaged in grids of $0.25° \times 0.25°$ (latitude $\times$ longitude). The mean count is converted to scaled radiance according to the prelaunch calibration table for the radiometer. Aging of the GMS-5/VISSR sensors is compensated by using a method developed by Kizu (2001). Cloud and land area are eliminated, and the brightness of sun glitter on the sea surface is obtained from the images. Cloud areas are detected by

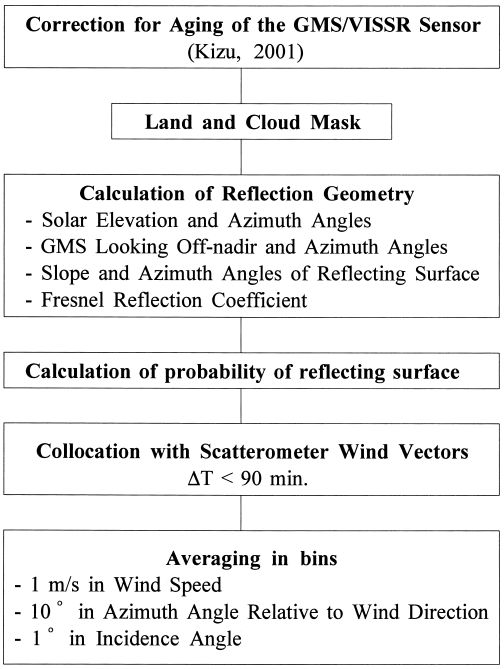

Fig. 2. Flowchart of data processing.

grid-averaged infrared brightness temperatures lower than 15°C.

Geometrical parameters, such as the solar elevation and azimuth angles, GMS looking off-nadir and azimuth angles, and slope and azimuth angle of the surface facets required for the reflection of the sun's ray toward GMS, are calculated for the center of each grid from the geometry of GMS observation and location of the sun. The Fresnel reflection coefficient is estimated from the slope angle. The brightness of the visible images is converted to the probability of wave surfaces which reflects the sunlight toward GMS by assuming that the brightness is proportional to the area of sea surface which reflects the sunlight. Only the primary scattering at the sea surface is considered, and scattering from the atmosphere is neglected.

The GMS images are then collocated with surface wind data observed by the three scatterometers. Temporal separation between the GMS and scatterometer observations are limited to within 90 min. Although we tried narrower time windows for the collocation (e.g., 60, 30, and 15 min.), the results showed no significant differences. The scatterometer vector fields of 50 km spatial resolution are linearly interpolated to the grid of 0.25° × 0.25° to be collocated with the GMS data.

Using the collocated data set of about 30 million points obtained in a period of about 4 years from 1995 to 1999, the probability distribution function of the surface slope was calculated as a function of wind speed, azimuth angle relative to the wind direction, and incidence angle in bins of 1 ms^{-1} in wind speed, 10° in azimuth angle, and 1° in incidence angle.

3. Results

Figure 3 shows the probability distribution of surface slope in the upwind/downwind and crosswind directions under various wind speeds. The upper panels show the mean and standard deviation of the probability distribution function (PDF) in arbitrary units, and the lower panels show the number of collocated data points used to calculate the probability distribution. The mean and standard deviation are calculated only where the number of data points exceeded 10. Outlyers which exceed three times the standard deviation were discarded and the mean and standard deviation were recalculated.

The distribution of data points is not uniform, representing the geometry of the sun and GMS observation and prevailing winds. In particular, there are few data points at normal incidence because of the geometrical constraints of the sun and GMS observation and the geographical location of islands in the western Tropical Pacific. The geographical distribution of data points is discussed in Section 4.

As expected, the probability decreases with the incidence angle. However, it does not reach zero even at high incidence angles. It is considered that scattering from the atmosphere and diffusive reflectors on the sea surface, such as whitecaps and bubbles, increases the reflection of sunlight and results in overestimation of the probability distribution function, which is assumed to be proportional to the brightness of sun glitter images (see Subsection 2.2). Assuming that these effects do not vary greatly with incidence angle, we utilized following equation to represent the probability function,

$$p(\theta) = a \exp(-\tan^2\theta/2\sigma^2) + b \qquad (1)$$

where p is the probability density function, θ is the incidence angle, σ is the root-mean-square (rms) slope, and a and b are constants. The value of σ, a and b are determined by the least-squares method. Thick lines in Fig. 3 are the fitted curves. The fitted curves represent the dependence of data points on incidence angle very well. No upwind/downwind asymmetry, as reported by Cox and Munk (1954a), is discernible, even under high winds.

Though the data are not shown here, the value of b is almost identical for all the cases and increases slightly with wind speed, implying the effects of whitecaps and bubbles. The atmospheric effect should also lead to positive bias of the probability density function, though its contribution may not be quantitatively evaluated in the presence of high and variable reflectance beneath the atmosphere. Errors in the GMS/VISSR calibration may also

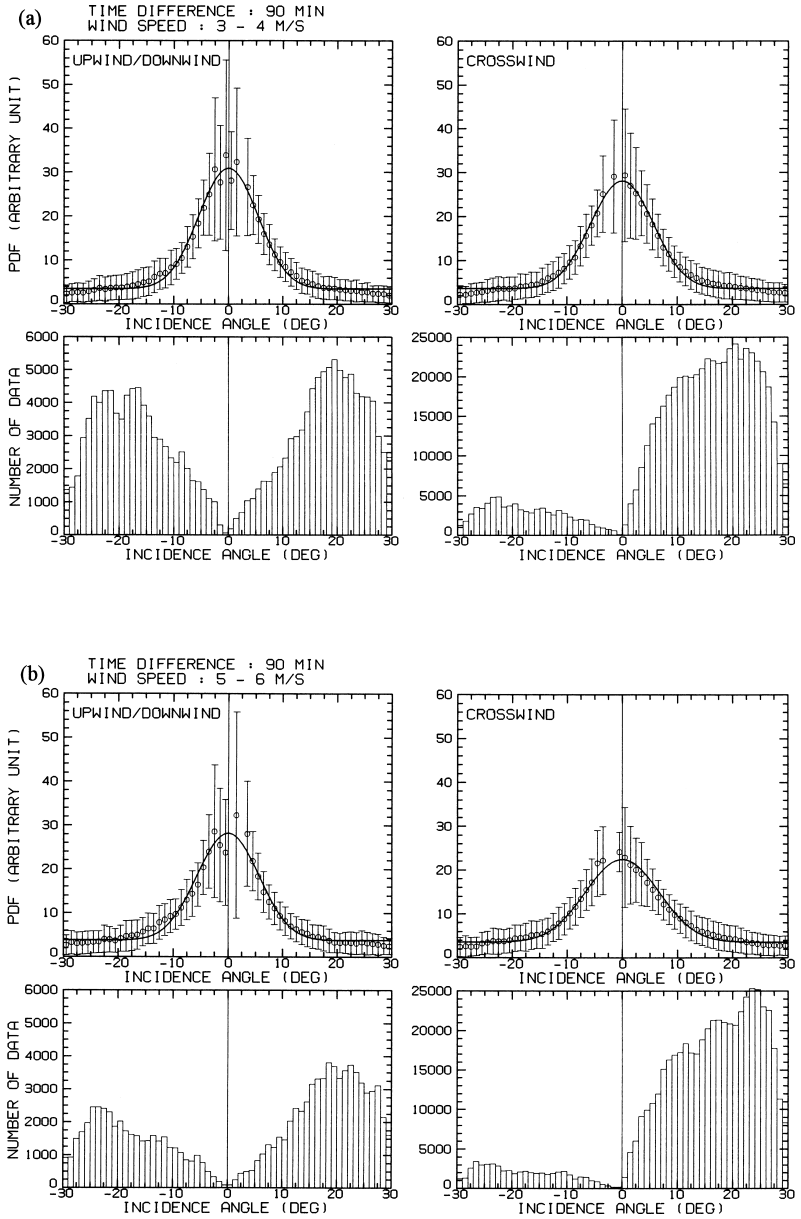

Fig. 3. Probability distribution of wave slope (upwind/downwind and crosswind directions) in an arbitrary unit (upper panels), and the number of collocated data points used to calculate the probability distribution (lower panels). (a) Wind speed of 3–4 ms^{-1}, (b) 5–6 ms^{-1}, (c) 7–8 ms^{-1}, and (d) 9–10 ms^{-1}.

contribute to the bias to some extent.

The variance of the surface slope components are plotted against wind speed in Fig. 4 (circles). Error bars indicate the 95% confidence interval of σ^2 using the least-squares fit to the data using Eq. (1). Thick lines represent the linear regression line on the data, expressed as,

$$\sigma_u^2 = 0.0053 + 6.71 \times 10^{-4}\, U_{10N}, \qquad (2)$$

$$\sigma_c^2 = 0.0048 + 1.52 \times 10^{-3}\, U_{10N}, \qquad (3)$$

and

$$\sigma_u^2 + \sigma_c^2 = 0.0101 + 2.19 \times 10^{-3}\, U_{10N}, \qquad (4)$$

for the upwind/downwind and crosswind components and the total slope, respectively, where U_{10N} is the neutral equivalent wind speed at a height of 10 m above the sea surface.

Thin solid and broken lines in Fig. 4 represent formulae proposed by Cox and Munk (1954a) for clean and

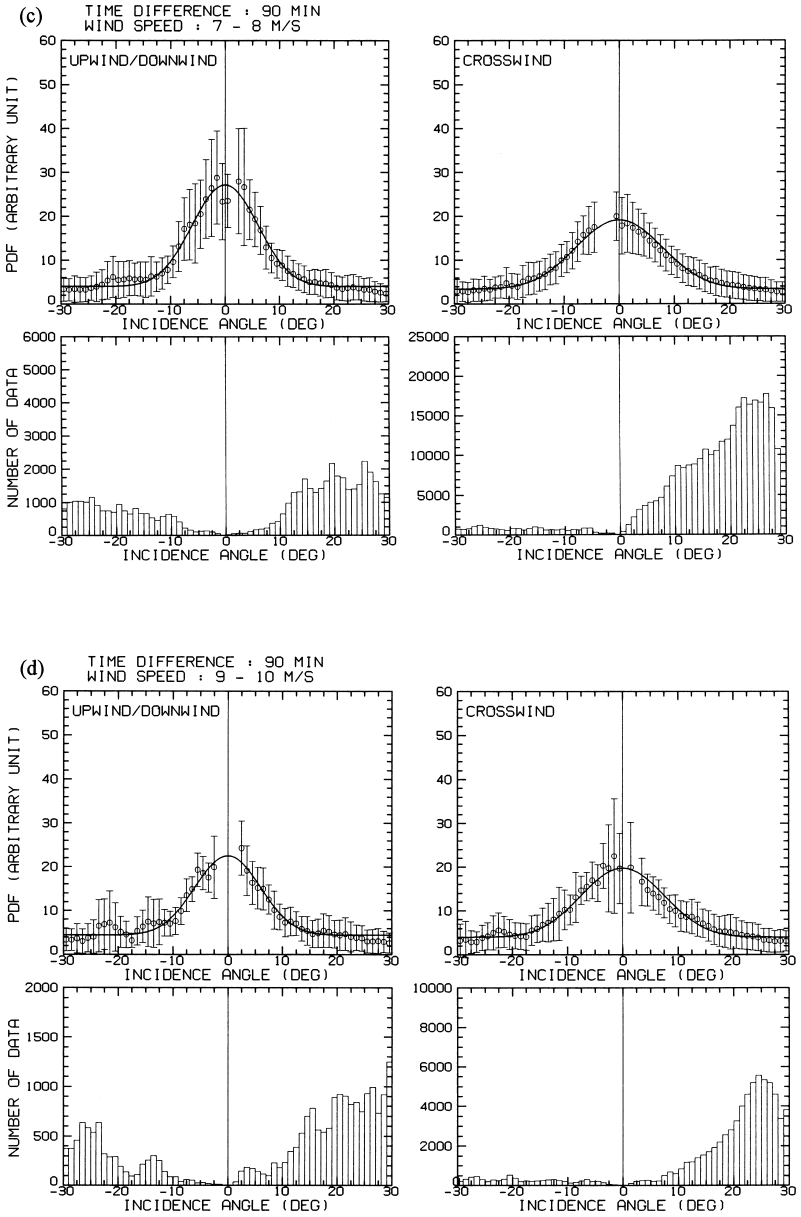

Fig. 3. (continued).

slick surfaces, respectively. Cox and Munk (1954a) used the observed wind speed at a height of 41 ft (12.5 m) above the sea surface. In Fig. 4, the wind speed is converted to that at a height of 10 m by multiplying by a constant of 0.918, which is equivalent to a value of the drag coefficient of 0.0015 under neutral stratification. No stability correction is made for the wind speed, since the observations by Cox and Munk (1954a, b) were made under near-neutral conditions and the stability effect is considered to be negligible.

Although the wind speed dependence of the cross-wind slope component agrees well with that of Cox and Munk (1954a), the upwind/downwind component is much lower. The surface slope estimated by the present method shows a narrower distribution and much less directivity relative to the wind direction than that reported by Cox and Munk (1954a).

4. Discussion

The results presented in the preceding section showed that the probability distribution of the surface slope has less asymmetry relative to the wind direction than that revealed by Cox and Munk (1954a). One possible reason is the difference in spatial resolution of the observation

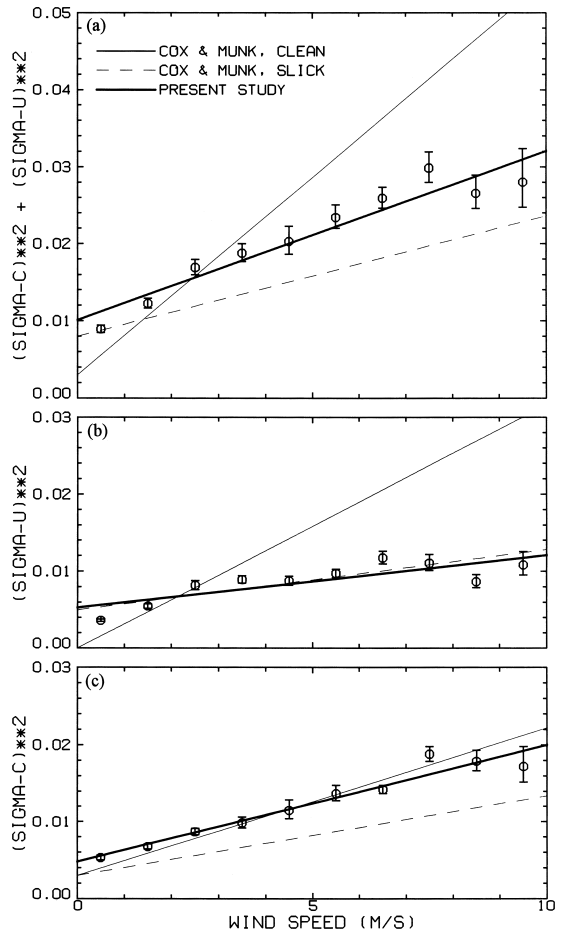

Fig. 4. Mean square slope components and their sum as functions of wind speed. (a) Total slope, (b) upwind/downwind, and (b) crosswind components. Error bars indicate 95% confidence intervals. Thick lines represents the linear regression line on the data. Thin solid and broken lines represent formulae proposed by Cox and Munk (1954a) for clean and slick surfaces, respectively.

techniques. Cox and Munk (1954a, b) took photographs of the sun glitter from aircraft flying at an altitude of 2000 ft (600 m), and the typical spatial scale of their observation is expected to be of the order of 1–10 m. By contrast, the spatial resolution of our data set is 0.25°. As suggested by Strong and Ruff (1970), variability of wind directions in the relatively large area over 0.25° × 0.25° to some extent may smear the directivity of slope distribution relative to the wind direction.

It is also expected that Cox and Munk (1954a, b) obtained their data under growing wind wave conditions, which is in equilibrium with the wind. In general, wind waves are not always developing, and the slope distribution might differ from their results (Donelan and Pierson, 1987; Hwang and Shemdin, 1988). This difference in conditions may be the reason for the difference of slope distribution.

Figure 5 shows (a) a histogram of wave age and (b) a comparison of wind and wave directions of the data utilized by Cox and Munk (1954a, b). The wave age, C_p/u_*, is defined by the ratio of phase speed of the dominant waves, C_p, and the friction velocity of the air, u_*. The phase speed is calculated from the significant wave period through the linear dispersion relationship of deep water waves, and the friction velocity is estimated using a formula of the drag coefficient proposed by Garratt (1977). Except for four data points, the directions of wind and waves agree with each other, and the wave age is lower than 30. This implies that the data of Cox and Munk were obtained under conditions of growing to fully-developed wind waves. According to Bailey *et al*. (1991), most of the wind and wave data observed under forcing of local wind show values of the wave age under 25.

Figure 6 shows the geographical distribution of (a) number of data points, and (b) mean wind speed of the data set used in the present study. Mean significant

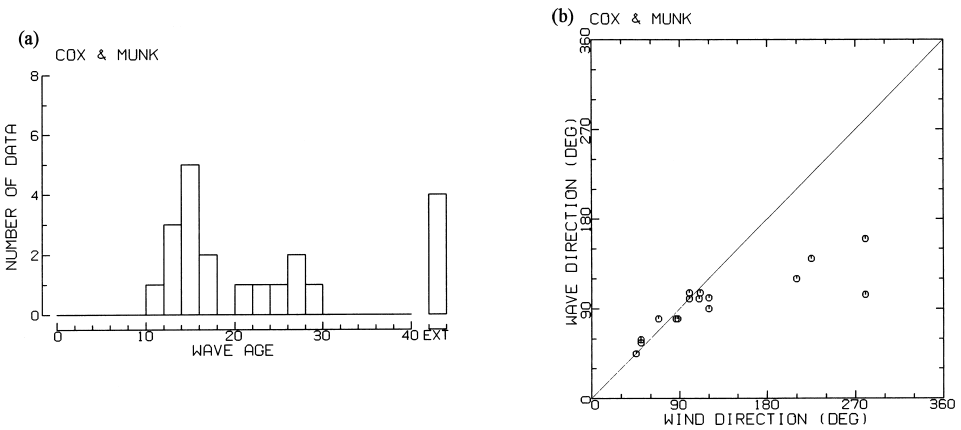

Fig. 5. (a) Histogram of wave age and (b) comparison of wind and wave directions of the data utilized by Cox and Munk (1954a, b). "EXT" implies values of wave age greater than 40.

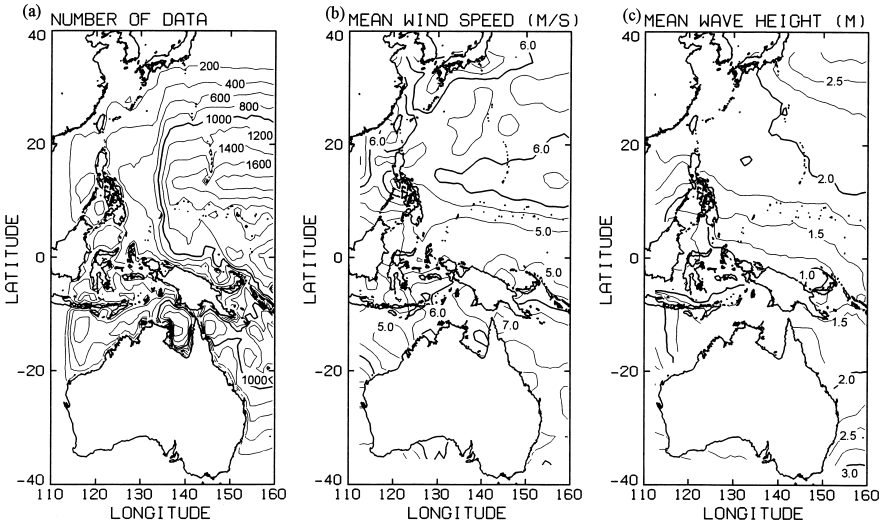

Fig. 6. (a) Geographical distribution of collocated data, (b) mean wind speed (ms^{-1}), and (c) mean significant waveheight (m).

waveheight (c) is estimated by collocating observations of the significant waveheight by the TOPEX/POSEIDON altimeter to the present data set. The significant waveheights observed along the satellite subtrack were averaged in grids of 0.25° × 0.25° and were collocated allowing time difference within 90 min. About 122,000 data points were collocated. This may be considered as random sampling from the whole data set of about 30 million data points, since the TOPEX/POSEIDON orbit is not sun-synchronous.

Most of the data were obtained in a region of subtropical high, as shown in Fig. 6(a). It is expected that swell is dominant in this region rather than growing wind waves. Since altimeters cannot measure wavelength (or wave period) and wave direction, we cannot discuss the maturity of the wind wave field using the wave age and wave direction relative to the wind direction as in Fig. 5.

In order to examine the difference of conditions of wave growth between the data sets of Cox and Munk and the present study, we use the non-dimensional waveheight defined as,

$$\hat{H} \equiv gH_{1/3} / U_{10}^2 \tag{5}$$

where g is the acceleration of gravity, $H_{1/3}$ is the significant waveheight, U_{10} is the wind speed. The relationship between the non-dimensional waveheight and fetch has been investigated for the purposes of wave modeling. For wind waves, the non-dimensional waveheight increases with the non-dimensional fetch and is saturated to 0.3 (Wilson, 1965; Ebuchi *et al.*, 1992; Ebuchi, 1999).

Figure 7 shows histograms of the non-dimensional significant waveheight of the data utilized by Cox and Munk (1954a, b) and the present study. Most of the Cox and Munk data points have values of the non-dimensional wave height around 0.1, implying that waves are growing under winds. In contrast to the data of Cox and Munk, a large portion of the present data set has a value of the non-dimensional significant waveheight larger than 0.3, implying that swells are dominant and waves are not expected to be in equilibrium with winds. It is considered that these differences in the conditions of wave growth caused the difference in slope distribution shown in Fig. 4. Swells propagating from various directions, which are

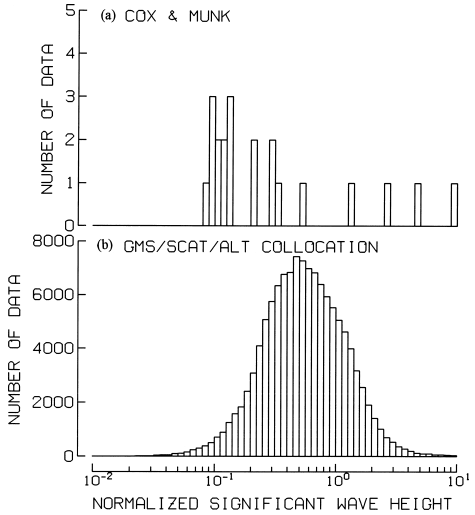

Fig. 7. Comparison of histograms of non-dimensional significant waveheight of the data utilized by (a) Cox and Munk (1954a, b), and (b) the present study.

independent of the local wind direction, result in the isotropic distribution of the surface slope. We believe the present data set represents a more general condition of wind waves over the global oceans than the limited data set of Cox and Munk (1954a, b). Bailey *et al*. (1991) discussed the relationship between the shape of wind waves and wave age. They concluded that younger wind waves are steeper and more asymmetric. Older waves approach a symmetric, sinusoidal form. This may explain the difference in upwind/downwind asymmetry of the surface slope. The results of the present study deduced from data obtained under a clear sky can be directly applicable to modeling the sea surface for optical remote sensing of the ocean, such as ocean color observations.

It might be suspected that errors in the ambiguity removal procedure of the scatterometer observations result in losing the upwind/downwind asymmetry of the slope distribution. The ambiguity removal is a procedure for selecting a unique solution from up to four initial wind vector solutions ("ambiguous" vectors) which are provided by the Maximum-Likelihood Estimation (MLE) wind retrieval (Naderi *et al*., 1991). Most of the cases for failure in ambiguity removal result in choosing a wind vector solution whose direction is almost opposite to the correct one. However, previous studies evaluating the skill of the ambiguity removal for the scatterometer wind products (e.g., Ebuchi *et al*., 1996, 1998; Graber *et al*., 1996; Ebuchi, 1999) reported that the probability of failure is less than 10% for wind speed greater than 5 ms^{-1}. Therefore, the failure of ambiguity removal may not be the reason for the loss of upwind/downwind asymmetry.

5. Application to an Altimeter Wind Model

We have tried to apply the present results to a wind model for radar altimeters. The normalized radar cross section (NRSC) is estimated from the probability density function of wave slope at vertical incidence by a specular scattering model according to Valenzuela (1978) and Donelan and Pierson (1987). The normalized radar cross section σ^0 is expressed as

$$\sigma^0(\theta) = \frac{|R(0)|}{\sigma^2} \sec^4\theta \exp\left(-\tan^2\theta / \sigma^2\right) \qquad (6)$$

where $R(0)$ is the Fresnel reflection coefficient for normal incidence, and σ^2 is the total variance of slope. The reflection coefficient $|R(0)|$ is given as

$$|R(0)| = |0.65(\varepsilon_r - 1)/(\varepsilon_r^{1/2} + 1)^2| \qquad (7)$$

where ε_r is the relative complex dielectric constant of the seawater, and is estimated according to Valenzuela (1981).

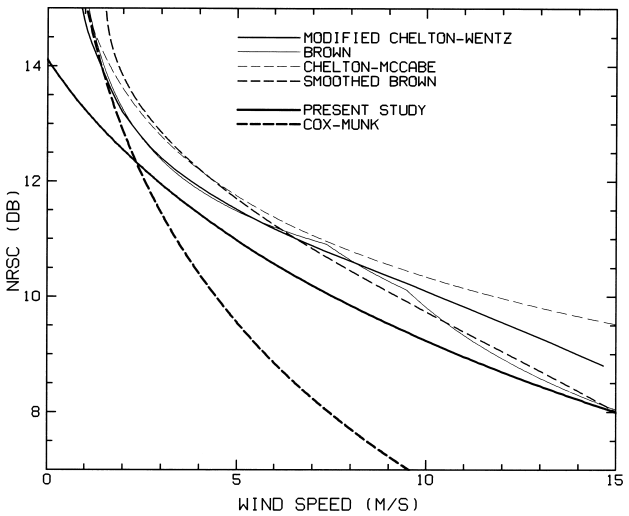

Fig. 8. Comparison of empirical model functions for altimeter wind with those derived from results of Cox and Munk (1954a, b) and the present study.

Figure 8 shows a comparison of empirical model functions for altimeter wind (Brown *et al*., 1981; Chelton and McCabe, 1985; Goldhirsh and Dobson, 1985; Witter and Chelton, 1991) with those derived from results of Cox and Munk (1954a) and the present study. The model function derived from the preset study is much closer to the empirical models than that from Cox and Munk in mid to high wind ranges. This result indirectly suggests that the surface slope variance estimated in the present study better represents the nature of the global ocean surface than that of Cox and Munk.

Although the model derived from the results of the present study represents the trend of radar cross section decreasing with wind speed closer to that of the empirical models, the absolute level is about 2 dB lower over the whole range of wind speed. One possible reason is that Eq. (6) ignores higher-order reflections, as discussed by Valenzuela (1978). Furthermore, the contribution to the slope variance from wavenumber components of the sea surface higher than the microwave wavenumber should be removed from the estimation of the radar cross section (Valenzuela, 1978; Donelan and Pierson, 1987). Jackson *et al*. (1992) discussed estimates of the scale separation wavenumber in detail. The present work has examined only the qualitative comparison of the estimated model function with that derived from the Cox and Munk formula. In order to construct a more realistic model for practical purposes, the effects of higher-order reflections and scale separation wavenumber will need to be considered.

6. Summary and Concluding Remarks

In the present study the probability distribution of the ocean surface slope has been estimated as a function of wind speed and azimuth angle relative to the wind direction using sun glitter images derived from GMS and surface vector winds observed by spaceborne scatterometers. The brightness of the visible images is converted to the probability of wave surfaces which reflect the sunlight toward GMS in grids of $0.25° \times 0.25°$ (latitude $\times$ longitude). Slope and azimuth angle required for the reflection of the sun's ray toward GMS are calculated for each grid from the geometry of GMS observation and location of the sun. The GMS images are then collocated with surface wind data observed by the three scatterometers. Using the collocated data set of about 30 million points obtained in a period of about 4 years from 1995 to 1999, the probability distribution function of the surface slope was obtained as a function of wind speed and azimuth angle relative to the wind direction.

The results were compared with those of Cox and Munk (1954a). The surface slope estimated by the present method shows a narrower distribution and much less directivity relative to the wind direction than that reported by Cox and Munk. It is expected that their data were obtained under conditions of growing wind waves. In general, wind waves are not always developing, and the slope distribution might differ from the results of Cox and Munk. Most of our data are obtained in the subtropical seas. Differences in the conditions may be the reason for the difference of slope distribution. The difference of maturity of wave growth was discussed using the nondimensional significant waveheight, estimated using observations of significant waveheight by the TOPEX/POSEIDON altimeter.

The symmetrical feature of wave slope relative to the wind direction might also be inconsistent with directional components in spectral models of the wind waves investigated in previous studies (e.g., Mitsuyasu *et al*., 1975; Hasselmann *et al*., 1980; Donelan *et al*., 1985). However, note that these studies were based on data obtained under conditions of growing wind waves. The distribution may largely depend on the maturity of wave growth, which has not been investigated and is not well understood.

The relationship between the variance of surface slope and wind speed has been applied to a wind model for altimeters. The derived model function is close to the empirical wind models. The results of the present study may also be applied directly to optical modeling of the sea surface and ocean color remote sensing. While the formulae proposed by Cox and Munk (1954a) represent the ocean surface slope under conditions of growing wind waves, the results of the present study are considered to represent average conditions over the global oceans.

Acknowledgements

The present study was partially supported by a Grant-in-Aid for Scientific Research (C) (project No. 11640424) from the Ministry of Education, Science, Sports, and Culture, Japan, and by the ADEOS-II Project from the National Space Development Agency of Japan (NASDA). The GMS-5/VISSR Histogram Data used in the present study were obtained from the Japan Meteorological Agency (JMA). The wind products from NSCAT, and ERS-1/2 were provided by the NASA Physical Oceanography Distributed Active Archive Center (PO.DAAC) at the Jet Propulsion Laboratory (JPL), California Institute of Technology, and Centre ERS d'Archivage et de Traitement (CERSAT), Institut Français de Recherche pour l'Exploitation de la Mer (IFREMER), respectively. The TOPEX/POSEIDON Altimeter Merged Geophysical Data Record (MGDR) were also provided by the NASA/JPL PO.DAAC. The authors are grateful to the data providers.

References

Bailey, R. J., I. S. F. Jones and T. Toba (1991): The steepness and shape of wind waves. *J. Oceanogr. Soc. Japan*, **47**, 249–264.

Bentamy, A., Y. Quilfen, P. Queffeulou and A. Cavanie (1994): Calibration of the ERS-1 scatterometer C-band model. Tech. Rep., IFREMER/Brest, DRO/OS-94-01, Brest, France, 72 pp.

Brown, G. S., H. R. Stanley and N. A. Roy (1981): The wind speed measurement capability of spaceborne radar altimeters. *IEEE J. Oceanic Eng.*, **OE-25**, 59–63.

Chelton, D. B. and P. J. McCabe (1985): A review of satellite altimeter measurement of sea surface wind speed: With a proposed new algorithm. *J. Geophys. Res.*, **90**, 4707–4720.

Cox, C. and W. H. Munk (1954a): Statistics of the sea surface derived from sun glitter. *J. Mar. Res.*, **13**, 198–227.

Cox, C. and W. H. Munk (1954b): Measurements of the roughness of the sea surface from photographs of the sun's glitter. *J. Opt. Soc. Am.*, **44**, 838–850.

Donelan, M. A. and W. J. Pierson (1987): Radar scattering and equilibrium ranges in wind-generated waves with application to scatterometry. *J. Geophys. Res.*, **92**, 4971–5029.

Donelan, M. A., J. Hamilton and W. H. Hui (1985): Directional spectra of wind waves. *Phil. Trans. R. Soc. London, Ser. A*, **315**, 509–562.

Ebuchi, N. (1999): Growth of wind waves with fetch in the Sea of Japan under winter monsoon investigated using data from satellite altimeters and scatterometer. *J. Oceanogr.*, **55**, 575–584.

Ebuchi, N., H. Kawamura and Y. Toba (1992): Growth of wind waves with fetch observed by the Geosat altimeter in the Japan Sea under winter monsoon. *J. Geophys. Res.*, **97**, 809–819.

Ebuchi, N., H. C. Graber and R. Vakkayil (1996): Evaluation of ERS-1 scatterometer winds with wind and wave ocean buoy observations. Tech. Rep., CAOS, Tohoku University, CAOS 96-001, Sendai, Japan, 69 pp.

Ebuchi, N., H. C. Graber, A. Bentamy and A. Mukaida (1998): Evaluation of NSCAT winds with ocean buoy observations. *Proc. PORSEC'98*, Qingdao, China, 396–400.

Freilich, M. H. and R. S. Dunbar (1999): The accuracy of the NSCAT-1 vector winds: Comparison with NDBC buoys. *J. Geophys. Res*., **104**, 11,231–11,246.

Garratt, J. R. (1977): Review of drag coefficients over oceans and continents. *Mon. Wea. Rev*., **105**, 915–929.

Goldhirsh, J. and E. D. Dobson (1985): A recommended algorithm for the determination of ocean surface wind using a satellite-borne radar altimeter. Tech. Rep. Appl. Phys. Lab., Johns Hopkins Univ., S1R85U-005, Laurel, MD, U.S.A.

Graber, H. C., N. Ebuchi and R. Vakkayil (1996): Evaluation of ERS-1 scatterometer winds with wind and wave ocean buoy observations. Tech. Rep., RSMAS, University of Miami, RSMAS 96-003, Miami, U.S.A., 69 pp.

Hasselmann, D. E., M. Dunkel and J. A. Ewing (1980): Directional wave spectra observed during JONSWAP 1973. *J. Phys. Oceanogr*., **10**, 1264–1280.

Hughes, B. A., H. L. Grant and R. W. Chappell (1977): A fast response surface-wave slope meter and measured wind-wave moments. *Deep-Sea Res.*, **24**, 1211–1223.

Hwang, P. A. and O. H. Shemdin (1988): The dependence of sea surface slope on atmospheric stability and swell conditions. *J. Geophys. Res*., **93**, 13,093–13,912.

Jackson, F. C., W. T. Walton, D. E. Hines, B. A. Walter and C. Y. Peng (1992): Sea surface mean square slope from Ku-band backscatter data. *J. Geophys. Res*., **97**, 11,411–11,427.

Khattak, S., R. A. Vaughan and A. P. Cracknell (1991): Sunlight and its observation in AVHRR data. *Remote Sens. Environ*., **37**, 101–116.

Kizu, S. (2001): An estimation of degradation of VISSR visible sensors aboard GMS-3, GMS-4, and GMS-5. *Int'l J. Remote Sens*. (in press).

Levanon, N. (1971): Determination of the sea surface slope distribution and wind velocity using sun glitter viewed from a synchronous satellite. *J. Phys. Oceanogr*., **1**, 214–220.

Long, S. R. and N. E. Huang (1976): On the variation and growth of wave slope spectra in the capillary-gravity range with increasing wind. *J. Fluid Mech*., **77**, 209–228.

Masuko, H., K. Arai, N. Ebuchi, M. Konda, M. Kubota, K. Kutsuwada, T. Manabe, A. Mukaida, T. Nakazawa, A. Nomura, A. Shibata and Y. Tahara (2000): Evaluation of vector winds observed by NSCAT in the seas around Japan. *J. Oceanogr*., **56**, 495–505.

Meteorological Satellite Center (1989): The GMS User's Guide. 2nd ed., Japan Meteorol. Agency, Tokyo, Japan, 222 pp.

Mitsuyasu, H., F. Tasai, T, Suhara, M. Ohkusu, T. Honda and K. Rikiishi (1975): Observation of the directional wave spectra of ocean waves using a cloverleaf buoy. *J. Phys. Oceanogr*., **5**, 750–760.

Naderi, F. M., M. H. Freilich and D. G. Long (1991): Spaceborne radar measurement of wind velocity over the ocean.—An overview the NSCAT scatterometer system. *Proc. IEEE*, **79**, 850–866.

Quilfen, Y. and A. Bentamy (1994): Calibration/validation of ERS-1 scatterometer precision products. *Proc. IGARSS'94*, Pasadena, U.S.A., 945–947.

Soules, D. S. (1970): Sun glitter viewed from space. *Deep-Sea Res*., **17**, 191–195.

Strong, A. E. and I. S. Ruff (1970): Utilizing satellite-observed solar reflections from the sea surface as an indicator of surface wind speeds. *Remote Sens. Environ*., **1**, 181–185.

Tang, S. and O. H. Shemdin (1983): Measurement of high frequency waves using a wave follower. *J. Geophys. Res*., **88**, 9832–9840.

Valenzuela, G. R. (1978): Theories for the interaction of electromagnetic and oceanic waves—a review. *Boundary-Layer Meteorol*., **13**, 61–85.

Valenzuela, G. R. (1981): Scattering of electromagnetic waves from the ocean. p. 199–226. In *Surveillance of Environmental Pollution and Resources by Electromagnetic Waves*, ed. by T. Lund, D. Reidel Pub. Co., Dordrecht, Holland.

Wald, L. and J. M. Monget (1983): Sea surface winds from sun glitter observations. *J. Geophys. Res*., **88**, 2547–2555.

Wilson, B. W. (1965): Numerical prediction of ocean waves in the North Atlantic for December, 1959. *Dtsch. Hydrogr. Z.*, **18**, 114–130.

Witter, D. L. and D. B. Chelton (1991): A Geosat altimeter wind speed algorithm and a method for altimeter wind speed algorithm development. *J. Geophys. Res*., **96**, 8853–8860.

Wu, J. (1971): Slope and curvature distributions of wind-disturbed water surface. *J. Opt. Soc. Am*., **61**, 852–858.

Wylie, D. P., B. B. Hinton and K. M. Millet (1981): Comparison of three satellite-based methods for estimating surface winds over ocean. *J. Appl. Meteorol*., **20**, 439–449.